Shock and Vibration 13 (2006) 577–593
IOS Press

Dynamic model of a rotating flexible arm-flexible root mechanism driven by a shaft flexible in torsion

S.Z. Ismail, A.A. Al-Qaisia* and B.O. Al-Bedoor**
Mechanical Engineering Department, Faculty of Engineering and Technology, University of Jordan, Amman 11942, Jordan

Received 23 July 2004
Revised 7 November 2005

Abstract. This paper presents a dynamic model of a rotating flexible beam carrying a payload at its tip. The model accounts for the driving shaft and the arm root flexibilities. The finite element method and the Lagrangian dynamics are used in deriving the equations of motion with the small deformation theory assumptions and the Euler-Bernoulli beam theory. The obtained model is a nonlinear-coupled system of differential equations. The model is simulated for different combinations of shaft and root flexibilities and arm properties. The simulation results showed that the root flexibility is an important factor that should be considered in association with the arm and shaft flexibilities, as its dynamics influence the motor motion. Moreover, the effect of system non-linearity on the dynamic behavior is investigated by simulating the equivalent linearized system and it was found to be an important factor that should be considered, particularly when designing a control strategy for practical implementation.

Keywords: Modeling, finite element, rotating, dynamic response, flexible arm, flexible root and flexible shaft

1. Introduction

Dynamic modeling of rotating flexible links has been the focus of extensive research efforts in the past two decades as an important tool for design and control purposes. In high-speed applications under lightweight constraints a comprehensive dynamic model that accounts for the arm flexibility and joint flexibilities is highly demanded for design, operations evaluation and control purposes. Previous models have succeeded in studying the effects of driving shaft/joint flexibility on the dynamic behavior of rotating flexible arms, such as presented by Al-Bedoor and Al-Mussalam [4]. A model that accounts for the arm root flexibility in addition to the driving joint flexibility is expected to be a more comprehensive model that can be used for more accurate dynamic behavior predictions and control applications.

Likins [13] reported a study on the mathematical modeling of spinning elastic bodies. A comparison between different modeling techniques like the simple concentrated model and the finite element method was reported. In the same direction, Kaza and Kvaternik [10], reported results of a study on the nonlinear flap-lag-axial equations of motion of a rotating beam. They have discussed the matter of inextensibility assumption when the effect of shortening is to be included. Yokohama [19], investigated the effect of shear deformations on the free vibrations characteristics of rotating beams. Chapnik et al. [6], reported a dynamic model for a rotating flexible arm impacted on its tip. They utilized the finite element method in discretizing the beam bending deformations and their model

*Corresponding author. E-mail: alqaisia@ju.edu.jo.
**On leave from King Fahd University of Petroleum and Minerals, Dhahran, Saudi Arabia.

ISSN 1070-9622/06/$17.00

resulted in a coupled dynamic model for the beam reference motion and the beam elastic deformations. Lee [12], studied the vibration of an inclined rotating beam with end mass. The effect of payload on the vibrations of a rotating beam was reported by Low [14]. The more general case, when the beam is sliding through a rotating hub, was reported by Al-Bedoor and Khulief [1–3]. In these studies general dynamic models that describe all rigid body motions and elastic deformations are reported. Most of these investigations were concerned with the arm flexibility and its effects on the overall performance of the manipulator and no attention to the joint flexibility was given.

The effects of joint flexibility on the dynamics and control of rigid manipulators was the concern of many investigators as can be seen in Spong [16]. In his work, Spong [16], modeled the joint flexibility as a torsional spring with more emphasis on simplifying the equations of motion for control purposes. Xi et al. [18], studied the coupling effects between the joint flexibility and the link flexibility using the system's natural frequencies. They offered two ratios, which are the inertia ratio and the stiffness ratio to quantify the coupling effect.

Recently, Huang and Ho [9], reported results of a similar study on the coupled shaft torsion and blade bending vibrations of a rotating shaft-disk-blade unit. The shaft-torsional and blade-bending deformations were modeled separately using the assumed modes method. They have used the weighted residual method and utilized the receptences at the connection between the disk and the blade to artificially couple the shaft-torsional and blade-bending deformations. The results of their study, in terms of natural frequencies and mode shapes, showed coupling between the blade and shaft and also coupling between the individual blades. Al-Bedoor and Al-Musallam [4], reported a study of a flexible-arm and flexible joint manipulator carrying a payload with rotary inertia. A finite element method is employed in deriving the equations of motion. All the dynamic coupling terms between the system reference rotational motions, joint torsional deformations and arm bending deformations are accounted for. The effects of the payload are shown to be increasing the elastic deformation amplitudes and reducing the frequency of oscillations. Garcia and Inman [7] proposed a model of the slewing control of a flexible structure. They generalized the boundary condition at the slewing axis to include the effect of the servo system. It is shown that the clamped-free beam assumption for the dynamics of the structure is a valid assumption if the ratio of the servo stiffness to beam flexibility is high. However, for moderate or low values of this ratio, the clamped boundary condition leads to erroneous system models so that it becomes necessary to consider the dynamic effects of the driving servo on the slewed beam.

In this paper a dynamic model of a rotating flexible link that is attached to a rigid hub with flexible root is developed. The rigid hub is driven through a shaft and compliant joint that makes the model accounting for all possible sources of flexibility and inertia. The arm model is developed using the finite element method and the Lagrangian dynamics. The model accounts for the payload dynamics and the effect of arm axial shortening. The model simulations using different parameters are presented in graphical forms and their results are discussed.

2. Dynamic model

The schematic diagram of a flexible arm driven by an electrical motor is shown in Fig. 1. The motor is assumed to have a rigid rotor with inertia J_m and rotating with angle θ_m. The Motor drives a shaft flexible in torsion modeled by torsional stiffness K_{ts}, which rotates the rigid hub with inertia J_h and rotates with an angle θ. Angles θ_m and θ are measured with respect to the inertial reference frame shown in Fig. 2. The arm is attached to the rigid hub using a torsional spring with stiffness K_t. The arm is modeled as a slender beam such that the effects of shear deformations and rotary inertia are neglected and the Euler Bernoulli beam theory is utilized. The arm is rotating in the horizontal plane and the gravitational forces are neglected. The coordinate systems used in developing the model are shown in Fig. 2. Wherein, XY is the inertial reference frame, $x_m y_m$ is a body coordinate system attached to the motor shaft and $x_h y_h$ is a body coordinate system attached to the hub such that its x_h axis is directed along the undeformed configuration of the arm. The arm is discretized using the finite element method as shown in Fig. 3. The arm is divided into n finite elements with the ith element having two nodes i and $i+1$. Each finite element has its own coordinate system xy attached to its first node i in its undeformed configuration. The position of the ith element coordinate system is defined by the position of the first node i in the $x_h y_h$ body axis. Using Lagrangian dynamics, which requires developing the kinetic and potential energy expressions, the model is developed in the following subsections.

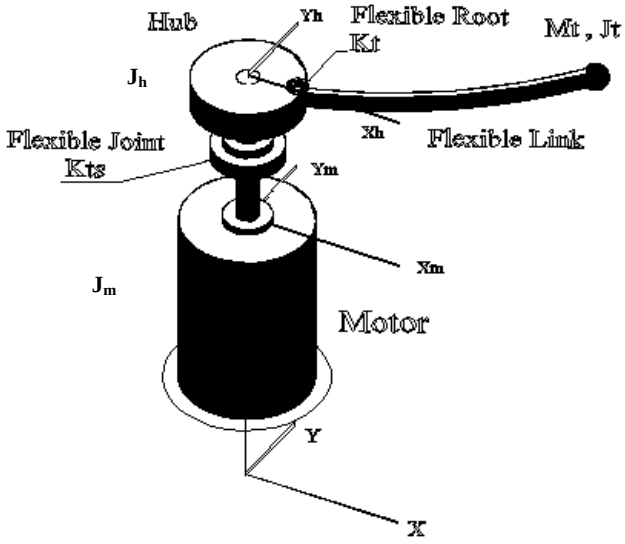

Fig. 1. Rotating flexible arm driven by a motor through a flexible joint.

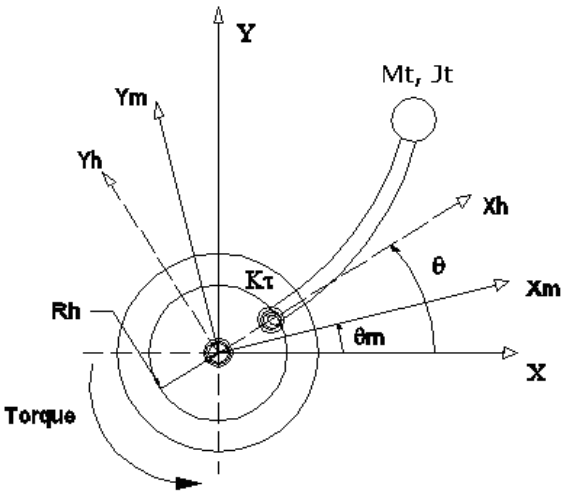

Fig. 2. Coordinate system.

2.1. Kinetic energy expression

The kinetic energy of the motor-hub-arm system is constituted of the arm, hub, motor and pay load kinetic energies. To obtain kinetic energy of the flexible rotating arm, the systematic approach of finding expression for the material velocity vector in the inertial reference frame is followed. The global position vector of a material p on the ith element of the beam can be written as:

$$R_p = [A(\theta)]\, r_p^h \tag{1}$$

where r_p^h is the position vector of point p in the hub coordinate system $x_h y_h$, $[A(\theta)]$ is the rotational transformation matrix from the hub coordinate system $x_h y_h$ to the *XY* inertial reference frame The position vector of point p in the $x_h y_h$ coordinate system can be expressed as

$$r_p^h = (S_i + x)\hat{i} + u(x,t)\hat{(j)} \tag{2}$$

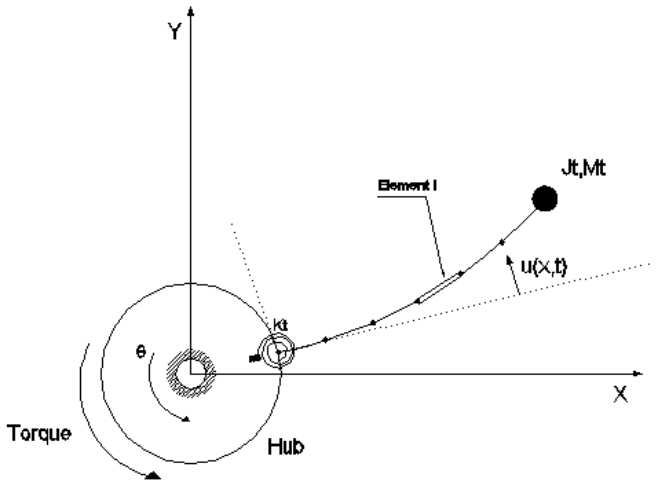

Fig. 3. Finite element discretization.

where $u\,(x,t)$ and S_i are the transverse elastic displacement of point p, and the axial position of node i measured relative to the $x_h y_h$ coordinate system, respectively. The rotational transformation matrices $[A\,(\theta)]$ can be represented in the following form

$$[A\,(\theta)] = \begin{bmatrix} \cos\theta & -\sin\theta \\ \sin\theta & \cos\theta \end{bmatrix} \tag{3}$$

where θ represents the hub angle measured relative to inertial reference frame. In order to formulate the kinetic energy of the arm, the velocity vector of the material point p can be obtained by differentiating Eq. (1) as follows

$$\dot{R}_p = \dot{\theta}\,[A_\theta\,(\theta)]\,r_p^h + [A\,(\theta)]\,\dot{r}_p^h \tag{4}$$

where $[A_\theta\,(\theta)]$ represents the derivative $dA/d\theta$.

The velocity vector in the hub coordinate system can be written as

$$\dot{r}_p^h = \dot{u}\,(x,t)\,\hat{j}^h \tag{5}$$

Now substituting for $[A\,(\theta)]$,$[A_\theta\,(\theta)]$ and $\dot{r}_p^h$ into Eq. (4), the velocity vector of point p in the inertial reference frame can be expressed in the following form

$$\dot{R}_p = \left\{ \begin{array}{l} -x_h\dot{\theta}\sin\theta - u\dot{\theta}\cos\theta - \dot{u}\sin\theta \\ x_h\dot{\theta}\cos\theta - u\dot{\theta}\sin\theta + \dot{u}\cos\theta \end{array} \right\} \tag{6}$$

where

$$x_h = S_i + x \tag{7}$$

The kinetic energy of a typical element i with mass per unit length ρ and length h can be written in the form

$$U_i = \frac{1}{2}\int_0^h \rho\, \overset{\bullet}{R}_p^{\,T}\, \overset{\bullet}{R}_p\, dx \tag{8}$$

substituting Eqs (6) and (7) into Eq. (8) leads to the element kinetic energy in the form

$$U_i = \rho h\left(S_i^2 + S_i h + \frac{1}{3}h^2\right)\overset{\bullet}{\theta}^{\,2} + \frac{1}{2}\int_0^h \rho\,\overset{\bullet}{\theta}^{\,2}\,u^2 dx + \int_0^h x_h\,\overset{\bullet\bullet}{\theta} u\,dx + \frac{1}{2}\int_0^h \rho\,\overset{\bullet}{u}^{\,2}\,dx \tag{9}$$

The kinetic energy expressions for the hub-shaft and motor, can be represented, respectively as

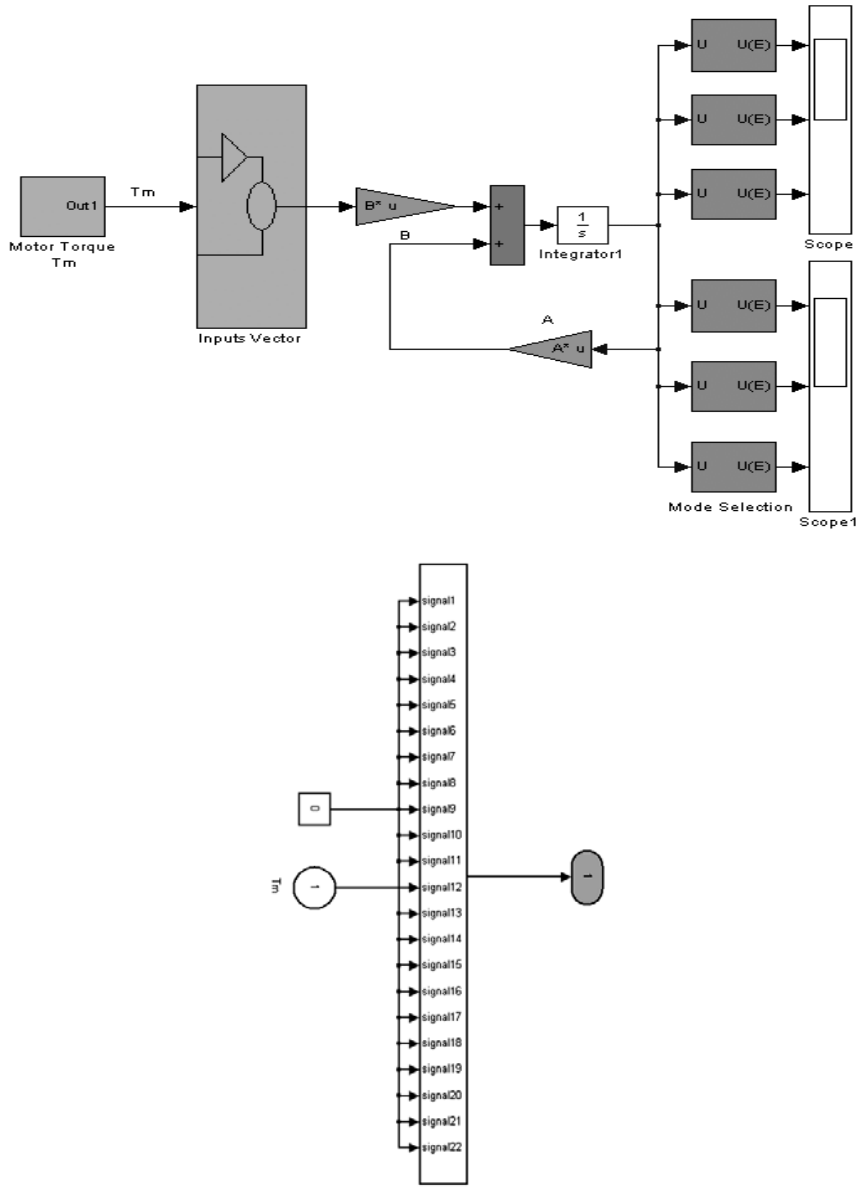

Fig. 4. Simulink of the linearized dynamic system.

$$U_h = \frac{J_h \dot{\theta}^2}{2}$$
$$U_m = \frac{J_m \dot{\theta}_m^2}{2} \tag{10}$$

where J_h and J_m are the hub and motor mass moment of inertia, respectively.

The system kinetic energy can be formed as

$$U = \sum_{i=1}^{n} U_i + U_h + U_m \tag{11}$$

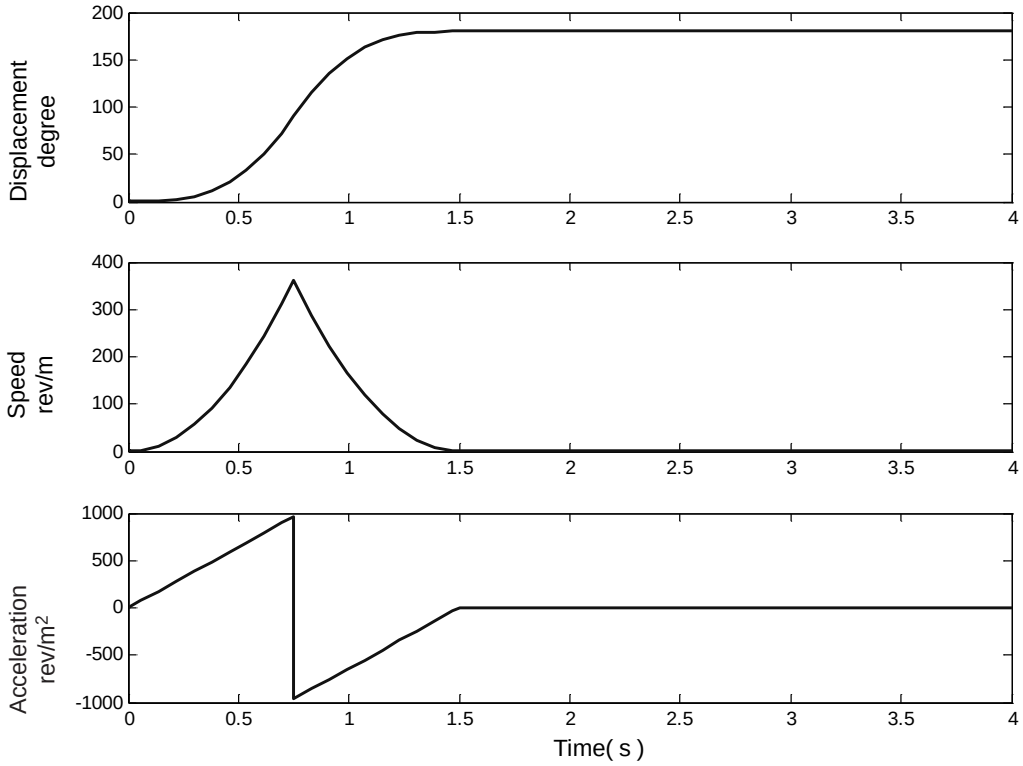

Fig. 5. Corresponding rigid body motion profile for the motion $\theta = \pi$ in 1.5 s, with linear acceleration.

where n is the number of elements. The remaining kinetic energy expression is that of the payload that is to be formulated in the section pertinent to the payload dynamics.

2.2. Potential energy expressions

The potential energy of the system consists of the elastic strain energy stored in the link, the arm root, shaft flexible joint and the potential energy stored in the axial shortening. The elastic strain energies stored in element i which has a flexural rigidity EI is known to have the form

$$V_{si} = \frac{1}{2}\int_0^h EI\left[\frac{\partial^2 u}{\partial x^2}\right]^2 dx \tag{12}$$

The torsional flexibility of the driving shaft stores strain energy that can be idealized by

$$V_{sj} = \frac{1}{2}K_{ts}\left(\theta_m - \theta\right)^2 \tag{13}$$

where K_{ts} is the torsional stiffness of the shaft, θ_m is the motor absolute angle of rotation and θ is the hub angle of rotation.

Finally, one last elastic energy storage element is the root torsional spring that can store energy of the form

$$V_r = \frac{1}{2}K_t u_1'^2 \tag{14}$$

where K_t is the torsional stiffness of the root attached spring and u' is the slope of the arm at the point of spring attachment.

The axial shortening due to transverse deformations in conjunction with the radial inertial forces result in a contribution to the system elastic potential energy known as the axial shortening potential energy [4], that can be

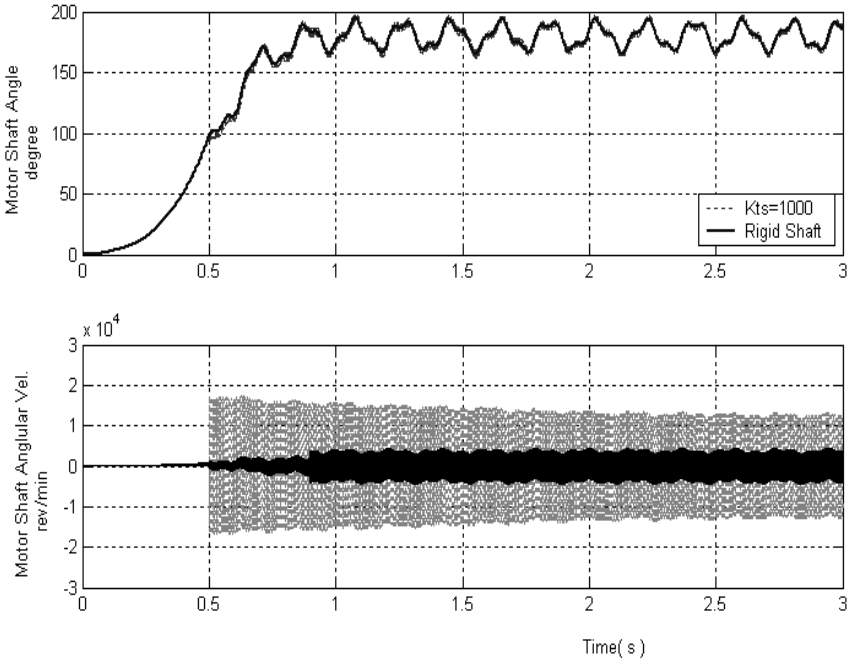

Fig. 6. Motor angular position and angular velocity for an arm with, $K_t = 1$ KN.m/rad, $L_b = 0.7$ m, carrying $m_T = 0.5$ kg.

represented in the form

$$V_{ai} = \frac{1}{2}\int_0^h \left[\rho\left(S_i \overset{\bullet}{\theta}^2 (h-x)\right) + \frac{1}{2}\overset{\bullet}{\theta}^2 \left(h^2 - x^2\right)\right]\left(\frac{\partial u}{\partial x}\right)^2 dx + \int_0^h \left[\sum_{j=i+1}^{n} \rho h\left(S_j + \frac{h}{2}\right)\dot{\theta}^2\right]\left(\frac{\partial u}{\partial x}\right)^2 dx \tag{15}$$

Now the total potential energy of the system can be expressed as

$$V = \sum_{i=1}^{n}\left(V_{ai} + V_{si}\right) + V_{sj} + V_r \tag{16}$$

2.3. Finite element discretization

The finite element method will be utilized to discretize the arm elastic deflection. In the finite element method, the deformations are usually represented in terms of the nodal degrees of freedom as

$$u(x,t) = [\phi(x)] \ \{q(t)\} \tag{17}$$

Where $[\phi]$ is a raw matrix of the shape functions which are spatially dependent and given by;

$$\phi_1(x) = 1 - \frac{3x^2}{h^2} + \frac{2x^3}{h^3}$$

$$\phi_2(x) = x - \frac{2x^2}{h} + \frac{x^3}{h^2}$$

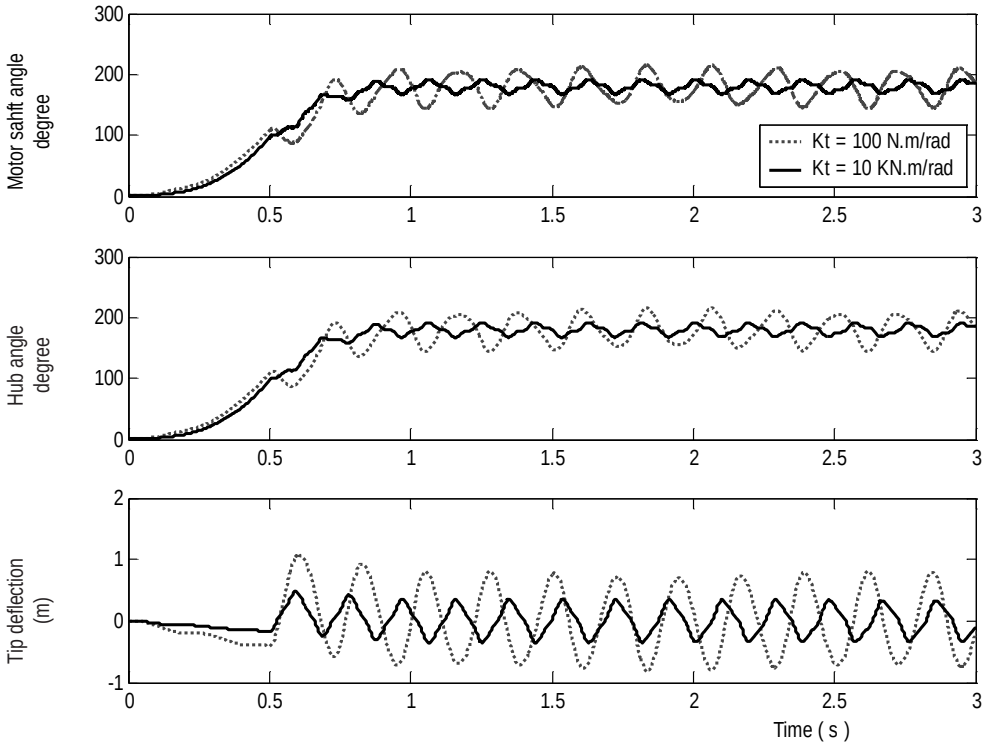

Fig. 7. Effect of root flexibility on system position responses $K_{ts} = 1000$ KN.m/rad, $L_b = 0.7$ m, $m_T = 0.5$ Kg.

$$\phi_3(x) = \frac{3x^2}{h^2} - \frac{2x^3}{h^3} \qquad (18)$$
$$\phi_4(x) = -\frac{x^2}{h} + \frac{x^3}{h^2}$$

and $\{q\}$ is the vector of nodal degrees of freedom which are time dependent. After substituting of Eq. (17) into Eq. (9) the element kinetic energy becomes

$$U_i = \frac{1}{2}\rho h\left(S_i^2 + S_i h + \frac{1}{3}h^2\right)\dot{\theta}^2 + \frac{1}{2}\dot{\theta}^2\{q\}^T\int_0^h \rho[\phi]^T[\phi]\,dx\,\{q\} + S_i\dot{\theta}\int_0^h \rho[\phi]\,dx\,\{\dot{q}\} + \dot{\theta}\int_0^h \rho x[\phi]\,dx\,\{\dot{q}\} + \frac{1}{2}\{\dot{q}\}^T\int_0^h \rho[\phi]^T[\phi]\,dx\,\{\dot{q}\} \qquad (19)$$

Similarly the bending strain energy and the axial shortening of element i, respectively, take the forms

$$V_{si} = \frac{1}{2}\int_0^h EI\left[\{q\}^T[\phi'']^T[\phi'']\{q\}\right]dx \qquad (20)$$

$$V_{ai} = \frac{1}{2}S_i\dot{\theta}^2\{q\}^T\int_0^h\left[\rho(h-x)[\phi']^T[\phi']\right]dx\,\{q\} + \frac{1}{4}\dot{\theta}^2\{q\}^T\int_0^h\left[\rho(h^2-x^2)[\phi']^T[\phi']\right]dx\,\{q\} + \frac{1}{2}\sum_{j=i+1}^{n}\rho h\left(S_j + \frac{h}{2}\right)\dot{\theta}^2\{q\}^T\int_0^h\left[\rho[\phi']^T[\phi']\right]dx\,\{q\} \qquad (21)$$

Performing the integrals of Eqs (19–21) using the Hermetian interpolation functions with uniform cross section result in the following constant coefficient matrices

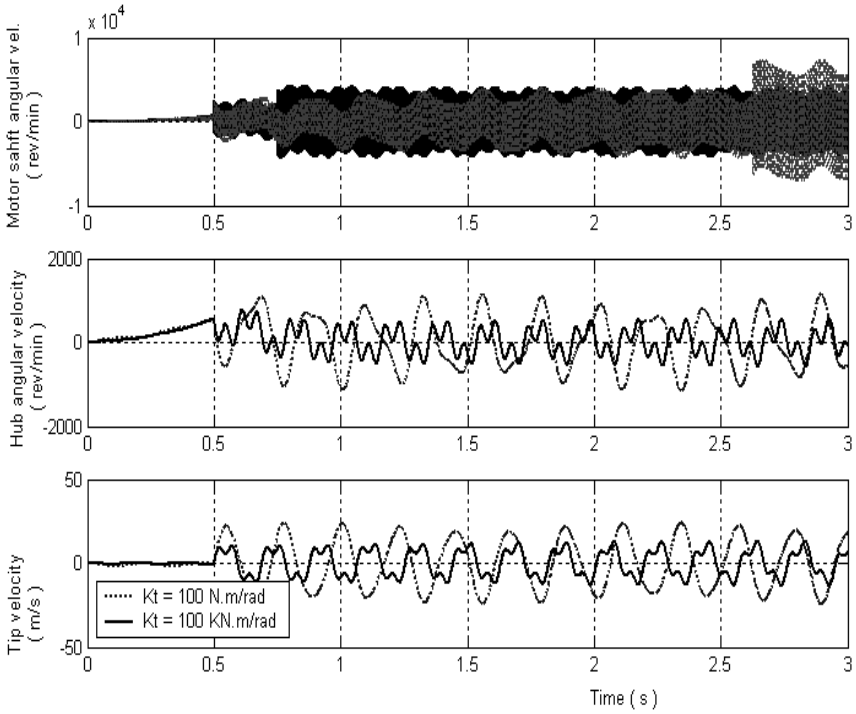

Fig. 8. Effect of root flexibility on system velocity responses, $K_{ts} = 1000$ KN.m/rad, $L_b = 0.7$ m, $m_T = 0.5$ Kg.

$$[M] = \int_0^h \rho \left[\phi\right]^T \left[\phi\right] dx = \frac{\rho h}{420} \begin{bmatrix} 156 & 22h & 54 & -13h \\ 22h & 4h^2 & 13h & -3h^2 \\ 54 & 13h & 156 & -22h \\ -13h & -3h^2 & -22h & 4h^2 \end{bmatrix} \tag{22}$$

$$[K] = \int_0^h EI \left[\phi''\right]^T \left[\phi''\right] dx = \frac{EI}{h^3} \begin{bmatrix} 12 & 6h & -12 & 6h \\ 6h & 4h^2 & -6h & 2h^2 \\ -12 & -6h & 12 & -6h \\ 6h & 2h^2 & -6h & 4h^2 \end{bmatrix} \tag{23}$$

$$[k_a] = \int_0^h \left[\rho \left(h - x\right) \left[\phi'\right]^T \left[\phi'\right]\right] dx = \frac{\rho}{60} \begin{bmatrix} 36 & 0 & -36 & 6h \\ 0 & 5h^2 & 0 & -h^2 \\ -36 & 0 & 36 & -6h \\ 6h & -h^2 & -6h & 2h^2 \end{bmatrix} \tag{24}$$

$$[k_b] = \int_0^h \left[\rho \left(h^2 - x^2\right) \left[\phi'\right]^T \left[\phi'\right]\right] dx = \frac{\rho}{210} \begin{bmatrix} 180h & 6h^2 & -180h & 27h^2 \\ 6h^2 & 24h^3 & -6h^2 & -4h^2 \\ -180h & -6h^2 & 180h & -27h^2 \\ 27h^2 & -4h^2 & -27h^2 & 10h^2 \end{bmatrix} \tag{25}$$

$$[k_c] = \int_0^h \rho \left[\phi'\right]^T \left[\phi'\right] dx = \frac{\rho}{30h} \begin{bmatrix} 36 & 3h & -36 & 3h \\ 3h & 4h^2 & -3h & -h^2 \\ -36 & -3h & 36 & -3h \\ 3h & -h^2 & -3h & 4h^2 \end{bmatrix} \tag{26}$$

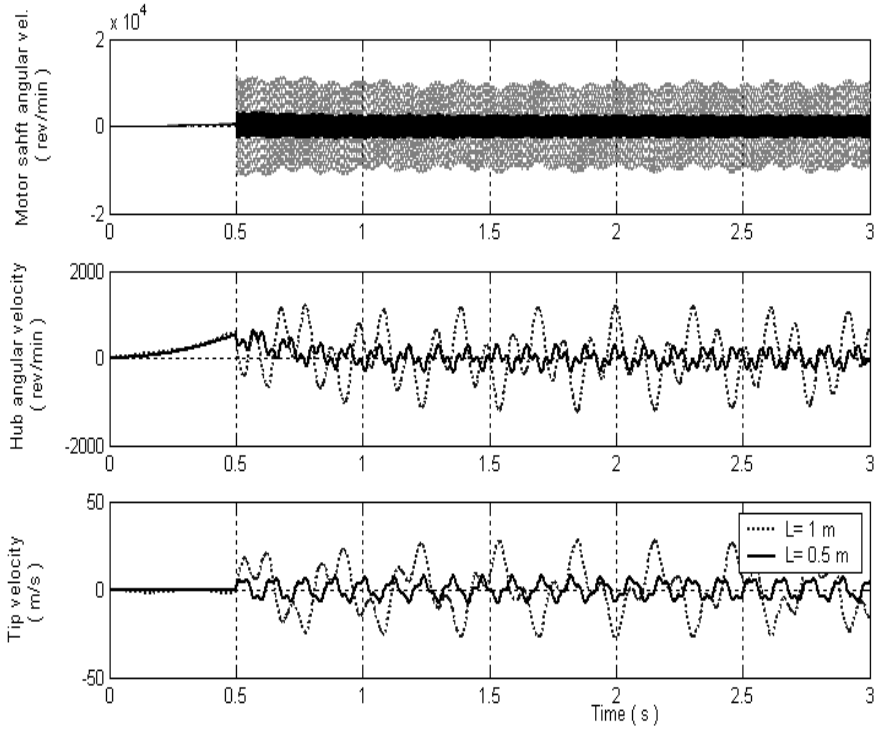

Fig. 9. Effect arm's length on system position responses $K_t = 10$ KN.m/rad, $K_{ts} = 10$ KNm/rad, $m_T = 0.5$ Kg.

$$[a] = \int_0^h \rho\,[\phi]\,dx = \frac{\rho l}{12}\begin{bmatrix}6 & h & 6 & -h\end{bmatrix} \tag{27}$$

$$[e] = \int_0^h \rho x\,[\phi]\,dx = \frac{\rho h^2}{60}\begin{bmatrix}9 & 2h & 21 & -3h\end{bmatrix} \tag{28}$$

Where the matrix $[M]$ is the consistent mass matrix that usually appears in the structural dynamics finite element formulations, $[K]$ is the conventional stiffness matrix. The matrices $[k_a]$, $[k_b]$ and $[k_c]$ result from the effect of axial shortening. The one-dimensional array $[a]$ and $[e]$ represent the coupling agents between the rigid angular motion and the elastic degrees of freedom. Upon substituting for the coefficient matrices, the system kinetic and potential energy expressions take the forms

$$\begin{aligned} U = \sum_{i=1}^{n} \Bigg[& \frac{1}{2}\rho h\left(S_i^2 + S_i h + \frac{1}{3}h^2\right)\dot{\theta}^2 + \frac{1}{2}\dot{\theta}^2\{q\}^T[M]\{q\} + \dot{\theta}\,[S_i\,[a] + [e]]\,\{\dot{q}\} \\ & + \frac{1}{2}\{\dot{q}\}^T[M]\{\dot{q}\}\Bigg] + \frac{1}{2}\left(J_d + J_{ds}\right)\dot{\theta}^2 + \frac{1}{2}\left(J_m + J_{ms}\right)\dot{\theta}_m^2 \end{aligned} \tag{29}$$

$$\begin{aligned} V = \sum_{i=1}^{n} \Bigg[& \frac{1}{2}\{q\}^T[K]\{q\} + \frac{1}{2}S_i\dot{\theta}^2\{q\}^T[k_a]\{q\} + \frac{1}{4}\dot{\theta}^2\{q\}^T[k_b]\{q\} \\ & + \frac{1}{2}\sum_{j=i+1}^{n} h\left(S_j + \frac{h}{2}\right)\dot{\theta}^2\{q\}^T[k_c]\{q\}\Bigg] + \frac{1}{2}K_{ts}\left(\theta_m - \theta\right)^2 + \frac{1}{2}K_t\dot{u}_1'^2 \end{aligned} \tag{30}$$

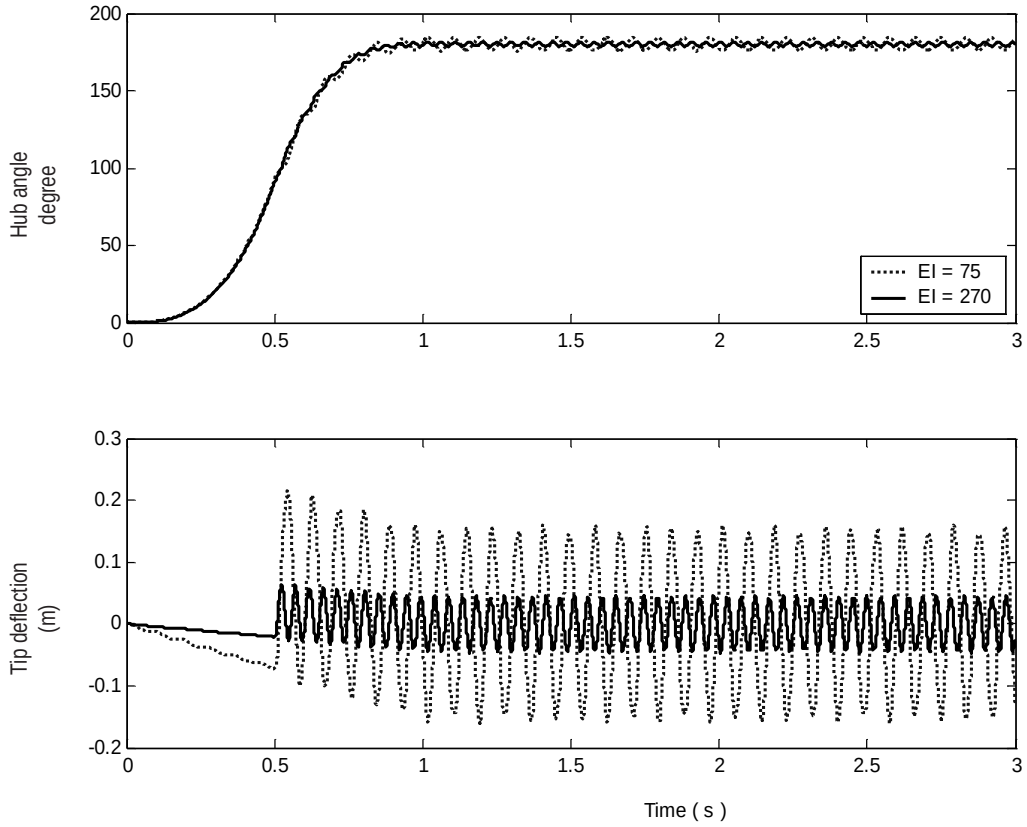

Fig. 10. Effect of flexural rigidity system position responses $K_t = 10$ KN.m/rad, $K_{ts} = 10$ KNm/rad, $L_b = 0.5$ m, $m_T = 0.5$ Kg.

The method of virtual work is adopted to formulate the external force vector of the model to be $\{F_{\theta m}, F_\theta, \{F_q\}\}$. Where $F_{\theta m}$ is the motor torque, F_θ is the torque applied to the hub and $\{F_q\}$ is the nodal forces at the arm equivalent discrete finite element model.

2.4. Equations of motion

Substituting the kinetic and potential energy expressions of Eqs (29) and (30) into the Lagrange's equation and after performing the needed differentiations and arrangement the system equations of motion can be represented in the following compact matrix form

$$\begin{bmatrix} M_{\theta_m\theta_m} & 0 & \vec{0} \\ 0 & M_{\theta\theta} & [M_{\theta q}] \\ \vec{0}^T & [M_{\theta q}^T] & [M_{qq}] \end{bmatrix} \begin{Bmatrix} \ddot{\theta}_m \\ \ddot{\theta} \\ \{\ddot{q}\} \end{Bmatrix} + \begin{bmatrix} D_v & 0 & \vec{0} \\ 0 & Q & \vec{0} \\ \vec{0}^T & \vec{0}^T & [0_{qq}] \end{bmatrix} \begin{Bmatrix} \theta_m \\ \theta \\ \{q\} \end{Bmatrix} + \begin{bmatrix} K_{ts} & -K_{ts} & \vec{0} \\ -K_{ts} & K_{ts} & \vec{0} \\ \vec{0}^T & \vec{0}^T & [K_R] \end{bmatrix} \begin{Bmatrix} \theta_m \\ \theta \\ \{q\} \end{Bmatrix} = \begin{Bmatrix} F_{\theta_m} \\ F_\theta \\ \{F_q\} \end{Bmatrix} \quad (31)$$

where

$$M_{\theta_m\theta_m} = (J_m) \quad (32)$$

$$M_{\theta\theta} = \left((J_d) + \sum_{i=1}^{n} \rho h \left(S_i^2 + S_i h + \frac{1}{3} h^2 \right) + \{q\}^T [M_{qq}] \{q\} \right) \quad (33)$$

$$[M_{\theta q}] = \sum_{i=1}^{n} (S_i [a] + [e]) \quad (34)$$

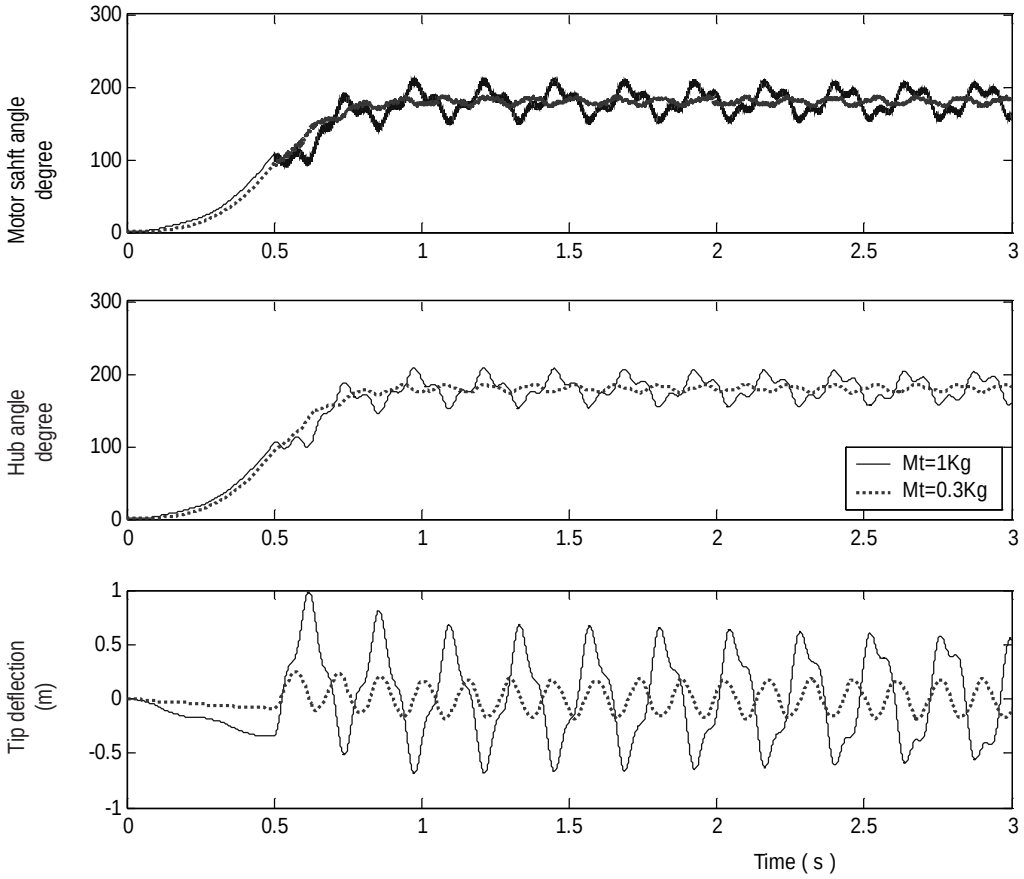

Fig. 11. Effect of payload on position responses, $K_t = 1000$ KN.m/rad, $K_{ts} = 1000$ KNm/rad, $L_b = 0.7$ m.

$$[M_{qq}] = \sum_{i=1}^{n} [M] \tag{35}$$

$$[K_R] = [K_{qq}] - \dot{\theta}^2 [M_{qq}] + f_1 \dot{\theta}^2 [k_{aqq}] + \frac{1}{2} \dot{\theta}^2 [k_{bqq}] + f_2 \dot{\theta}^2 [k_{cqq}] \tag{36}$$

$$f_1 = \sum_{i=1}^{n} S_i \tag{37}$$

$$f_2 = \sum_{i=1}^{n} \left(\sum_{j=i+1}^{n} h \left(S_j + \frac{h}{2} \right) \right) \tag{38}$$

Where $\vec{0}^T$ is a zero vector of size $(1 \times n)$ and D_v is the damping coefficient in the electrical motor. Equation (31) represents the dynamics of rotating flexible arm, hub, and motor system. The degrees of freedom of this system are the motor and rigid hub angular rotations θ_m and θ, respectively, and the arm nodal degrees of freedom $\{q\}$ vector. The entry $M_{\theta_m \theta_m}$ is the rotational inertia of the motor, $M_{\theta\theta}$ is the rotational inertia of the hub and the arm and $[M_{qq}]$ is the arm generalized global elastic mass matrix. The entry $M_{\theta q}$ represents the nonlinear inertia coupling between the hub reference rotational motion and the arm bending deformations. The matrix $[K_{qq}]$ is the generalized stiffness matrix, which is shown to be affected by the reference rotation. The right-hand-side of Eq. (31) represents the vector of external forces and moments.

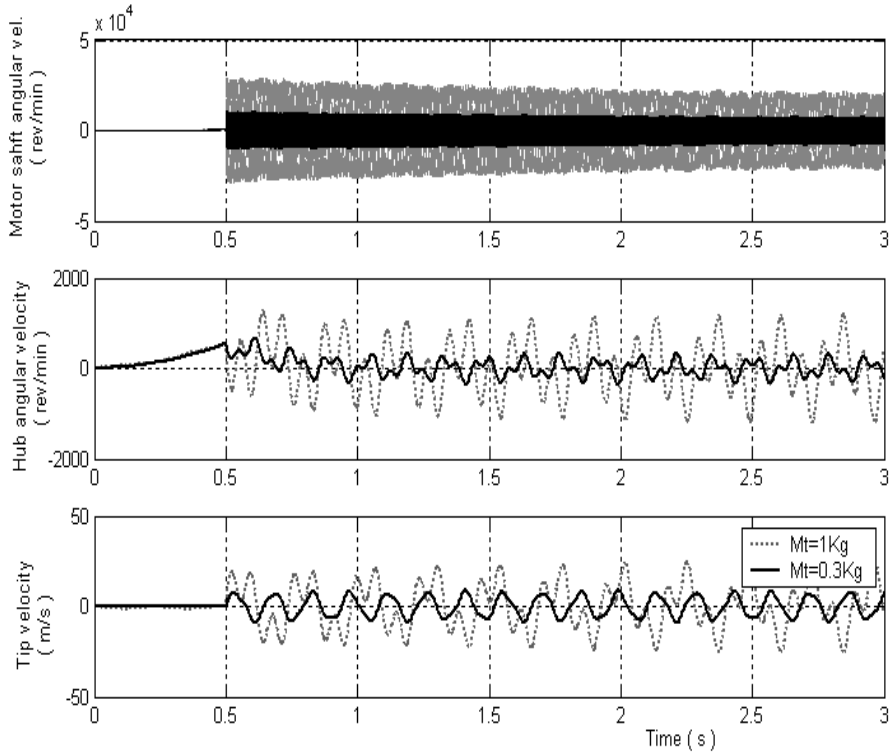

Fig. 12. Effect of payload on velocity responses, $K_t = 1000$ KN.m/rad, $K_{ts} = 1000$ KNm/rad, $L_b = 0.7$ m.

For comparison purposes and to get more information about the dynamic behavior of the system, the model that resulted in equation (31) is linearized about zero deflection for both joint torsional deformation and the link bending deformations and is written as;

$$\begin{bmatrix} M_{\theta_m\theta_m} & 0 & \vec{0} \\ 0 & M_{\theta\theta} & [M_{\theta q}] \\ \vec{0}^T & [M_{\theta q}]^T & [M_{qq}] \end{bmatrix} \begin{Bmatrix} \ddot{\theta}_m \\ \ddot{\theta} \\ \{\ddot{q}\} \end{Bmatrix} + \begin{bmatrix} D_v & 0 & \vec{0} \\ 0 & 0 & \vec{0} \\ \vec{0}^T & \vec{0}^T & [0_{qq}] \end{bmatrix} \begin{Bmatrix} \dot{\theta}_m \\ \dot{\theta} \\ \{\dot{q}\} \end{Bmatrix} + \begin{bmatrix} K_{ts} & -K_{ts} & \vec{0} \\ -K_{ts} & K_{ts} & \vec{0} \\ \vec{0}^T & \vec{0}^T & [K_R] \end{bmatrix} \begin{Bmatrix} \theta_m \\ \theta \\ \{q\} \end{Bmatrix} = \begin{Bmatrix} F_{\theta_m} \\ F_\theta \\ \{F_q\} \end{Bmatrix} \quad (39)$$

Where

$$M_{\theta\theta} = \left((J_d) + \sum_{i=1}^{n} \rho h \left(S_i^2 + S_i h + \frac{1}{3} h^2 \right) \right) \quad (40)$$

$$[K_R] = [K_{qq}] \quad (41)$$

3. Payload dynamics

The payload, as shown in Fig. 1, is located at the tip of the arm. After defining the velocity vector of the payload, finding its corresponding kinetic and potential energy contributions, the payload equations of motion can be represented in the following form

$$\begin{bmatrix} M_{11}^t & M_{12}^t \\ M_{21}^t & M_{22}^t \end{bmatrix} \begin{Bmatrix} \ddot{\theta} \\ \ddot{u}_L \\ \ddot{u}'_L \end{Bmatrix} + \begin{Bmatrix} 2m_T u_L \dot{u}_L \dot{\theta} \\ (S_L - 1)\, m_T \dot{\theta}^2 u_L \\ 0 \end{Bmatrix} = \begin{Bmatrix} 0 \\ 0 \\ 0 \end{Bmatrix} \quad (42)$$

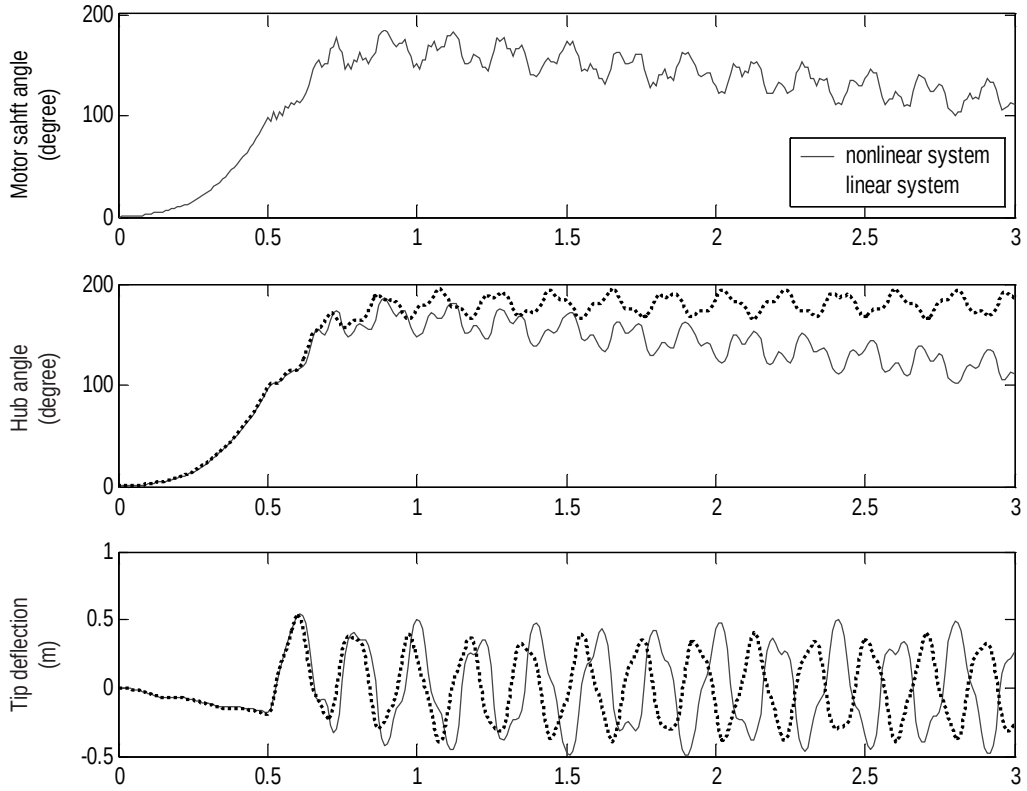

Fig. 13. Linear and nonlinear system position responses. $K_t = 10$ KN.m/rad, $K_{ts} = 10$ KN.m/rad, $= 0.7$ m, $m_T = 0.5$ Kg

Where u_L is the position of the pay load at the last node in the finite element mesh and the entries of Eq. (42) can be detailed as follows

$$M_{11}^t = m_T L^2 + J_T + m_T u_L^2 \tag{43}$$

$$M_{12}^t = \begin{bmatrix} m_T L \; J_T \end{bmatrix} \tag{44}$$

$$M_{21}^t = {M_{21}^t}^T \tag{45}$$

$$M_{22}^t = \begin{bmatrix} m_T & 0 \\ 0 & J_T \end{bmatrix} \tag{46}$$

Now, the entire of the equations of motion of the payload, Eq. (42), are to be added to the corresponding entries of the equations of the motion of the whole system. By looking at the equations, it is revealed that the payload is contributing to the nonlinear dynamic interaction between the link rigid body rotation and its elastic deflection degrees of freedom. Furthermore, the proposed model of the payload can be used for any location along the arm span, provided that a nodal point is assigned at the payload location. Consequently, the payload axial position along the arm and its transverse deflection are taken as the corresponding node axial position and transverse defection, respectively.

The equation of motion of the payload given in Eq. (42) is linearzied and given by the following equation;

$$\begin{bmatrix} M_{11}^t & M_{12}^t \\ M_{21}^t & M_{22}^t \end{bmatrix} \begin{Bmatrix} \ddot{\theta} \\ \ddot{u}_L \\ \ddot{u}_L' \end{Bmatrix} + = \begin{Bmatrix} 0 \\ 0 \\ 0 \end{Bmatrix} \tag{47}$$

Where

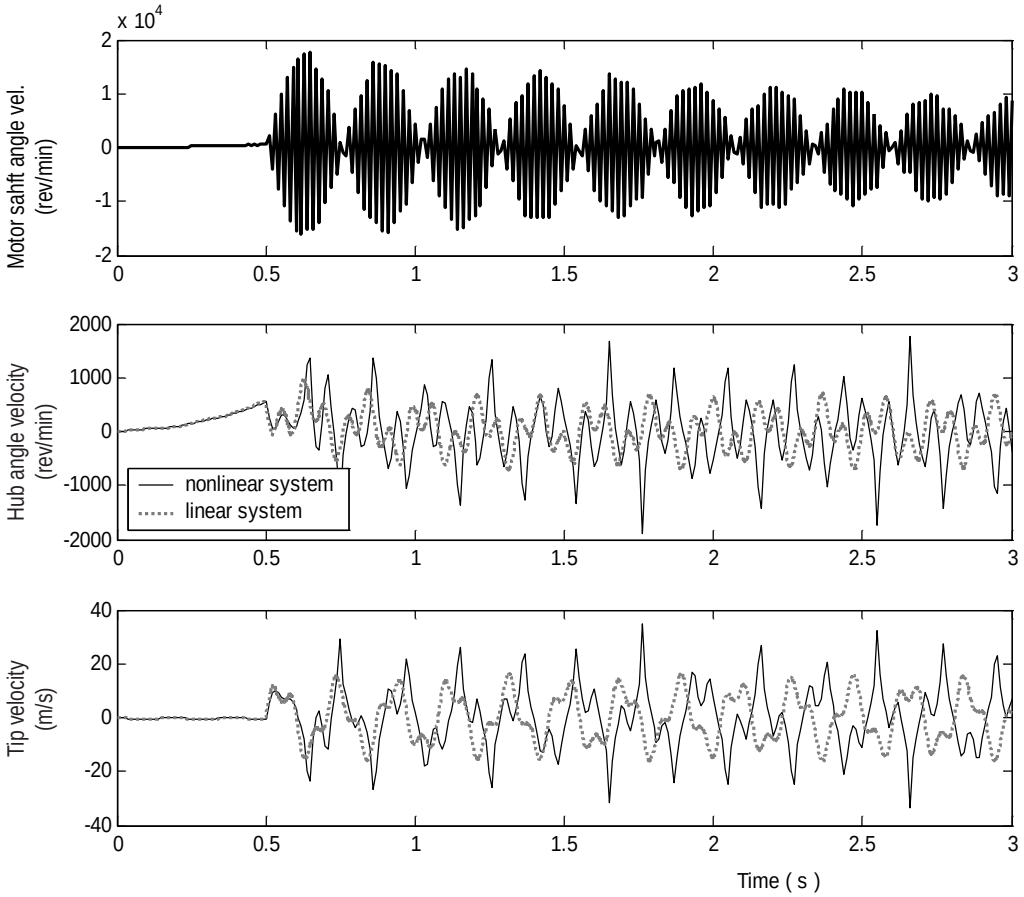

Fig. 14. Linear and nonlinear system velocity responses $K_t = 10$ KN.m/rad, $K_{ts} = 10$ KN.m/rad, $L_b = 0.7$ m, $m_T = 0.5$ Kg.

$$M_{11}^t = m_T L^2 + J_T \tag{48}$$

The other entries are the same as given in Eqs (44–46).

4. Numerical simulations

The developed nonlinear dynamic model, Eqs (31) and (42), has been set for computational purposes using two main processors. The first processor is the finite element module in which the invariant structural dynamic matrices and vectors are calculated. The second processor receives the invariant matrices for a particular problem and formulates the system of nonlinear second-order equations that include the rigid body reference motions and the arm nodal degrees of freedom. The system of second-order equations is then numerically converted into a system of first-order equations to perform time marching integration using the predictor-corrector algorithm. The ode45 of the MATLAB package and Simulink are used in the simulations. Figure 4 shows the Simulink model for the system that consists of subsystem blocks connected to each other to represent the dynamic system. For simulations purposes, a uniform arm made of aluminum with the dimensions and material properties given in Table 1 is used.

In this model, one should remember that the system consists of a motor rotor, rotating with angle θ_m, connected to the rigid hub that rotates with angle θ, where the hub carries the flexible arm that also carries on its tip the payload. The driver is the motor that will produce a torque on its own rotor and finally drives the hub-arm-payload assembly. Using the inverse dynamic procedure and based on the rigid body model, the torque that is required to rotate the system to a specified target angular position in a specified maneuvering time can be calculated. For this rigid body

Table 1
Flexible Arm- Hub- motor data

Property	Symbol	Value range
Arm length	L_b	0.4–1.5 m
Mass per unit length	ρ	1.35 Kg/m
Cross section		100 mm $\times$ 5 mm
Flexural rigidity	EI	75–270 Nm^2
Hub diameter	D_h	100 mm
Hub length	L_h	150 mm
Hub moment of inertia	J_h	3.94 $\times$ 10^{-3} kg.m^2
Hub shaft length	L_{hs}	33 mm
Motor shaft length	L_{ms}	400 mm
Motor shaft diameter	D_{ms}	33 mm

system the angular position of the motor rotor, the hub and the arm is the same as no flexibility is involved. For the present numerical example, the torque that is required to rotate the arm an angle $\theta = \pi$ in 1.5 seconds and the corresponding rigid body angular position, velocity and acceleration are calculated and given in Fig. 5.

The first parameter to be investigated is the effect of the motor-hub shaft flexibility on the motion of the motor. Figure 6 shows the motor angular position and motor angular velocity for the cases when the shaft connecting the motor and the hub is rigid and flexible. As shown, the angular position of the motor is slightly affected, however, the fluctuation of the motor angular velocity due to shaft flexibility is pronounced. This result supports the finding of Al-Bedoor [4]. To study the effect of the arm root flexibility of the system dynamics, an example is simulated for two values of the root flexibility. The simulation results are shown in Figs 7 and 8, for angular positions and velocities, respectively. As shown, and despite that the flexible root is attached to the hub, the effect of its flexibility is reflected in the motor angular position and angular velocity. Moreover, abrupt changes in the motor velocity can be observed which indicate that the combined effect of shaft flexibility and root flexibility can play an important role in the motor dynamics and stability in the form of dynamic coupling that needs further investigation. The effects of arm parameters such as the arm length and arm flexural rigidity can be investigated using the model as shown Figs 9 and 10. As shown, the arm length and flexural rigidity play similar roles as the arm length is reduced, the increase in flexural rigidity that result in reducing the vibration amplitude and increasing the vibration frequency.

The effect of payload on the dynamics of a rotating flexible arm with flexible shaft and flexible root is investigated by considering two values of the payload. The simulation results are compared in Figs 11 and 12, for the position and velocity variations, simultaneously. For control purposes, some theories require linearization steps. To investigate the effect of linearization on the dynamic behavior of the simulated system, Eqs (39) and (47) are solved and the results are compared for the position and velocity variations of the motor-hub-arm system. The linear and nonlinear systems show different responses in terms of the motor angular position and velocity as well as on the tip deflection amplitudes and frequencies. This indicates that linearization should be done with care when designing control schemes for practical implementation.

5. Conclusions

A dynamic model for a rotating flexible arm carrying a payload is developed. The model differs from previously reported models by considering the flexibilities of the driving shaft and the arm root flexibility. The finite element method was used in conjunction with the Lagrangian dynamics in deriving the equations of motion that were presented in compact matrix form. The model depends on the Euler-Bernoulli beam theory and the effect of axial shortening and payload dynamics are accounted for. The simulation results showed that the arm root flexibility plays an important role in the predicted dynamic behavior of the rotating arm and its effects reflect back to the motor motion and consequently caution should be taken when designing a vibration control is designed for such rotating arms.

Acknowledgments

The authors acknowledge the support of the University of Jordan and King Fahd University of Petroleum and Minerals.

References

[1] B.O. Al-Bedoor and Y.A. Khulief, Vibrational motion of an elastic beam with prismatic and revolute joints, *Journal of Sound and Vibration* **190**(2) 1996, 195–206.

[2] B.O. Al-Bedoor and Y.A. Khulief, Finite element dynamic modeling of translating and rotating flexible link, *Computer Methods in Applied Mechanics and Engineering* **131** (1996), 173–189.

[3] B.O. Al-Bedoor and Y.A. Khulief, General planar dynamics of a sliding flexible link, *Journal of Sound and Vibration* **206**(5) (1997), 641–661.

[4] B.O. Al-Bedoor and A.A. Almusallam, Dynamics of flexible-link and flexible-joint manipulator carrying a payload with rotary inertia, *Mechanism and Machine Theory* **35** (1999), 785–820.

[5] L.W. Chang, *Dynamic Analysis Of Robotics Manipulators With Flexible Links*, Ph.D. Thesis, Purdue University, 1984.

[6] B. Chapnik, G. Heppler and J. Aplevich, Modeling impact on a one link flexible robot arm, *IEEE Transactions on Robotics and Automation* **7**(4) (1991), 479–488.

[7] E. Garcia and D. Inman, Modeling of the slewing control of a flexible structure, *AIAA, Journal of Guidance, Control and Dynamics* **14**(4) (1991), 736–742.

[8] M. Geradin, G. Robert and G. Bernardin, Dynamic modeling of manipulators with flexible members, in: *Advanced Software in Robotics*, A. Dantiline and M. Geradin, eds, Elsevier, North-Holland, 1984, pp. 27–39.

[9] S. Huang and K. Ho, Coupled shaft-torsion and blade-bending vibrations of a rotating shaft-disk-blade unit, *Journal of Engineering for Gas Turbines and Power* **118** (1996), 100–106.

[10] K. Kaza and R. Kvaternik, Nonlinear flap-lag-axial equations of a rotating beam, *AIAA Journal* **15**(6) (1977), 871–874.

[11] Y.W. Kwon and H. Bang, *The Finite Element Method Using MATLAB*, CRC Press, Washington, DC, 1997, 235–299.

[12] H. Lee, Vibration on an inclined rotating cantilever beam with tip mass, *Journal of Vibration and Acoustics* **115** (1993), 241–245.

[13] P.W. Likins, F.J. Barbera and V. Baddeley, Mathematical modeling of spinning elastic bodies for modal nalysis, *AIAA Journal* **11**(9) (1973), 1251–1258.

[14] K.H. Low, Vibration analysis of a top-loaded beam attached to a rotating joint, *Computers and Structures* **52**(5) (1994), 955–968.

[15] G. Naganathan and A.H. Soni, Non-linear flexibility studies for spatial manipulators, *Proceedings of the 1986 IEEE International Conference on Robotics and Automation* **1** (1986), 373–378.

[16] M.W. Spong, Modeling and control of flexible joint robots, *Journal of Dynamic Systems, Measurements and Control* **109** (1987), 310–319.

[17] W.H. Sunada and S. Dubowsky, On the dynamic analysis and behavior of industrial robotic manipulators with elastic members, *ASME Journal Of Mechanism, Transmission, Automation And Design* **105** (1983), 42–50.

[18] F. Xi, R.G. Fenton and B. Tabbarok, Coupling effects in a manipulator with both flexible link and joint, *Journal of Dynamic Systems, Measurements and Control* **116** (1994), 826–831.

[19] T. Yokohama, Free vibration characteristics of rotating timeshenko beams, *International Journal of Mechanical Science* **30**(10) (1988), 743–755.